Chen, An; Yossef, Mostafa; Hopkins, Paul

A comparative study of different methods to calculate degrees of composite action for insulated concrete sandwich panels

Published in:
Engineering Structures

DOI:
10.1016/j.engstruct.2020.110423

Published: 01/06/2020

Document Version
Peer-reviewed accepted author manuscript, also known as Final accepted manuscript or Post-print

A COMPARATIVE STUDY OF DIFFERENT METHODS TO CALCULATE DEGREES OF COMPOSITE ACTION FOR INSULATED CONCRETE SANDWICH PANELS

An Chen[1], Mostafa Yossef[2*] and Paul Hopkins[3]

Abstract

Precast concrete sandwich wall panels consist of two outer wythes of precast concrete separated by a middle layer of insulation. In recent years, Fiber-Reinforced Polymer (FRP) shear connectors have been increasingly used since they have lower thermal conductivity compared to traditional steel shear connectors, which can significantly reduce thermal bridging. However, FRP shear connectors have lower stiffness, resulting in partial Degree of Composite Action (DCA), which is an important parameter to describe the structural behavior of the panels. Different methods have been proposed to calculate DCAs, including displacement method, strain method, and load method. This paper will compare and evaluate the effectiveness of these methods. A bending test was conducted on a full size of 7 m x 3 m, precast, prestressed insulated concrete sandwich panel with FRP shear connectors. A non-linear Finite Element (FE)

[1] Professor, Department of Building Engineering, School of Civil Engineering, Beijing Jiaotong University, Beijing, China.
[2] *Assistant Professor, Arab Academy for Science and Technology and Maritime Transport, Cairo, Egypt, , and Postdoctoral Researcher, Aalto University, Espoo, Finland myossef@aast.edu (corresponding author).
[3] Vice President, TD&H Engineering, Media, PA 19063, USA.

model is created, where good correlations can be achieved between the test and FE results. The FE model is further employed to conduct a parametric study by varying the stiffness of the shear connectors. DCAs for different stiffnesses are calculated using the aforementioned three methods and the applicability and limitation of each method are investigated.

Keywords: Insulated Concrete Sandwich Panel, Partial Degree of Composite Action; Strain Method; Displacement Method; Load Method.

1. Introduction

Precast, prestressed insulated concrete sandwich panels consist of two outer layers of precast concrete separated by a middle layer of insulation, usually using expanded polystyrene (EPS) or extruded polystyrene (XPS), as shown in Figure 1. These panels can provide strength and protect the interior of the building from thermal gradients by separating the thermal bridge in the concrete panel with the insulation layer. They can be used as wall (vertical) and roof/floor (horizontal) panels.

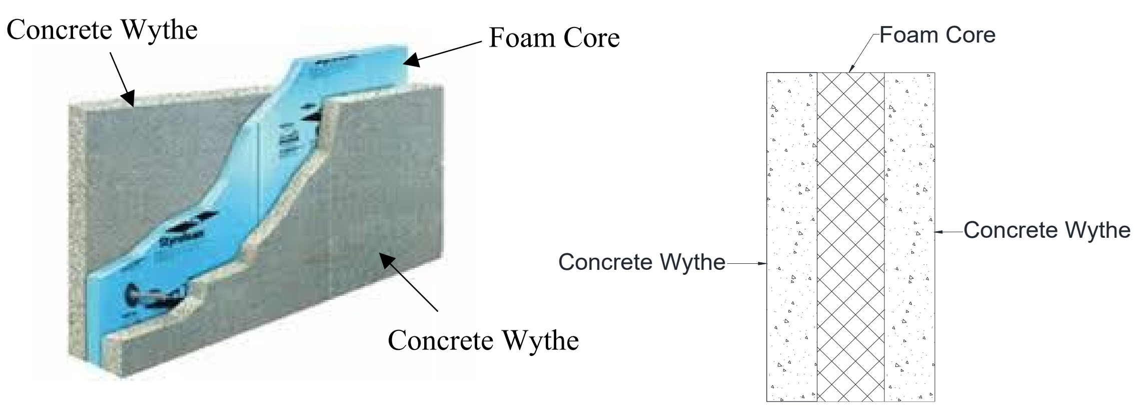

(a) 3-D view (b) Section View

Figure 1 Concrete sandwich panel

Since the two outer layers of the panels are separated, they need to be connected by shear connectors in order for the panels to provide composite action. Steel shear connectors have been commonly used since 1990s, including small bent bars, steel wire trusses, and continuous bent bars [(Bush and Stine 1994; Bush and Wu 1998; Einea et al. 1991)]. However, steel has a high thermal conductivity which can cause thermal bridging. Also, it is susceptible to corrosion. To address these limitations, Fiber-Reinforced Polymer (FRP) shear connectors have been developed, since they have much lower thermal conductivity compared to steel and do not corrode, which can increase the lifetime of the structure.

FRP composites have higher tensile strength but a rather low shear strength. Therefore, FRP connectors should be properly arranged to introduce tensile and compressive stresses in FRP composites and avoid shear stress. The applicability of using different types of FRP shear connectors in sandwich panels have been studied in the past. Einea et al. (1994) introduced hybrid steel/FRP connectors where FRP connectors were used as the diagonal members of the truss web and the top and bottom chords were prestressing strands. Full-scale tests and 2-D FE analysis were conducted. Salmon et al. (1998) tested four full-scale sandwich panels, two panels with FRP bent bars and the other two with steel connectors. They found that the FRP connectors could improve the thermal insulation of the sandwich panel. The strength of each panel is equal to that of a full-composite panel.

Whitehead and Ibell (2005) investigated the performance of the aramid FRP as transverse reinforcement for concrete beams using unbonded rectangular and circular helixes. They concluded that the unbonded rectangular helixes were 50% less effective than fully bonded helixes. Frankl et al. (2011) tested six full-scale precast, prestressed sandwich panels with carbon FRP (CFRP) shear connectors. They concluded that the CFRP shear connectors could achieve full-composite action. Three different configurations of glass FRP (GFRP) were used as shear connectors for sandwich panels and tested by the first author's research group [Chen et al. (2015)]. They used continuous, segmental and discrete FRP shear plates, where the continuous and segmental connectors had better performance than the discrete connectors. Choi et al. (2015) studied the sandwich panels with GFRP grid shear connectors subjected to wind pressure and suction using positive and negative loading. Tomlinson and Fam (2015) investigated the performance of the sandwich panels using basalt FRP (BFRP).

Generally, shear connectors can be classified into stiff and flexible shear connectors. In contrast to steel, most types of FRP shear connectors can be treated as flexible shear connectors where limited slip is permitted between the outer wythes. Therefore, it is essential to study the slip between the concrete wythes for sandwich panels with FRP connectors.

The slip occurring in the sandwich panels can be defined using the concept of "Degree of Composite Action (DCA)". The percentage of composite action that a sandwich panel can exhibit is an important engineering design parameter. In some cases, the panel can be conservatively considered as non-composite and only one of the outer wythes is used to take the axial or flexural load. However, in many cases, the sandwich panel, which contains concrete wythes at each side connected with some form of shear tie, will exhibit a percentage of composite action.

Until now, there is no uniform method to determine DCA. Bush and Stine (1994), Tomlinson and Fam (2018), Cox et al. (2019) and Al-Rubaye et al. (2019) used the moment of the panel to calculate DCA, which were calculated from the section modulus and the average strain difference. Pessiki and Mlynarczyk (2003), Choi et al. (2015) and O′Hegarty et al. (2019) defined DCA based on the theoretical value of the moment of inertia. Frankl et al. (2011), Chen et al. (2015) and Joseph et al. (2017) calculated DCA based on the deflection at selected loads. This method can be termed as “deflection method”.

Tomlinson and Fam (2015) calculated DCA based on the ultimate load. They compared DCA based on load vs. DCA and deflection vs. DCA; and concluded that the load method can be used at the ultimate stage based on the ultimate load while the deflection method can be used during serviceability limit state. This method can be termed as “load method”.

Lorenz and Stockwell (1984) defined DCA based on strain for the concrete deck on steel beams. Full composite (100% DCA) assumes no slip between the beam and concrete slab, while non-composite (0% DCA) assumes a full slip between the beam and concrete slab. Similarly, partial DCA can occur when there is a partial slip between the beam and concrete slab. The same concept can be adopted for sandwich panels. This method can be termed as “strain method”. Details of the three methods will be provided in Section 5.

The first author’s group studied the effect of DCA on the behavior of sandwich panels with general configuration flexible shear connectors using shear lag model (Yossef and Chen, 2018). They found that DCA has a significant effect on the stress/strain induced in the sandwich panels. They further developed a simplified model to calculate stresses and deflections for different DCAs, which could be used for design. Since DCA can significantly affect the structural performance of the panel, there is a need to describe the

DCA accurately. The objective of this paper is to compare the three methods shown above for panels with FRP shear connectors and evaluate their applicability and limitations. A bending test on a full-scale sandwich panel with FRP shear connectors was conducted and a nonlinear Finite Element (FE) model was constructed, as described next.

2. Experimental Investigation

The sandwich panel was manufactured in accordance with American Concrete Institute (ACI) and Precast, Prestressed Concrete Institute (PCI) specifications and tested by Hopkins (2015). The panel was 3 m x 7 m x 0.25 m (width x length x thickness), which was constructed on a flat horizontal bed, as shown in Figure 1. Truss grid connectors were installed to connect the two concrete wythes. They were placed in the form and concrete, when poured, interlocked between openings in the connector truss elements. The spacing of the three connectors was 1.22 m. Six 9.5 mm diameter with grade 270 prestressing strands were spaced equally at 559 mm at the top and bottom of the panel, as shown in Figure 3, and were set at 75% of peak stress, which was equivelant to 76.5 kN prestressing force. The wire mesh was a smooth wire 102x102-MW13.3/13.3, where "102x102" was the spacing of the strands in millimeters and "MW" referred to Metric Wire with a cross-section area of 13.3 mm^2. CFRP shear connector consisted of grids with a spacing of 40.7 mm and 45.7 mm in the longitudinal and transverse direction, respectively. The shear mesh was rotated 45 degrees to obtain the maximum benefit of the grid to carry the shear load, as shown in Figure 10. Material properties are shown in Table 1. Detailed properties of the CFRP shear connectors are provided in Table 2.

Table 1 Material properties

Material	Concrete	Insulation	Steel Wire	Prestressing Strand	CFRP Grid (Long.)	CFRP Grid (Trans.)
Strength (MPa)	54	-	466 (yield) 597 (ultimate)	1389 (yield) 1954 (ultimate)	2000	1758
Young's Modulus (GPa)	29	3.30E-03	200	190	255	186
Poisson's Ratio (ν)	0.15	0.35	0.3	0.3	0.3	0.3
Density (Kg/m^3)	2403	29	7850	7850	1000	1000

Table 2 Material properties of CFRP shear connectors

Shear grid type	Longitudinal Properties				Transverse Properties			
CFRP shear connector	A (mm^2/m)	f_u (GPa/m)	E (GPa)	ε_u (%)	A (mm^2/m)	f_u (GPa/m)	E (GPa)	ε_u (%)
	41.04	2	253	0.76	45.4	1.76	180	0.76

2.1 Test setup

The test panel was laid flatwise and supported on two 14 cm x 14 cm wood blocks as shown in Figure 4. The loading applied consisted of precast concrete ecology blocks, which were placed on the panel as shown in Figure 4 and Figure 5, sequentially with an approximate 10 minutes gap between the block placement to simulate typical floor loading. Deflections were recorded after each block was applied using both survey equipment and a dial gauge at the midspan, as shown in Figure 4. The blocks were later weighed individually to obtain their exact weight.

Figure 2 Sandwich panel production prior to placing top concrete wythe

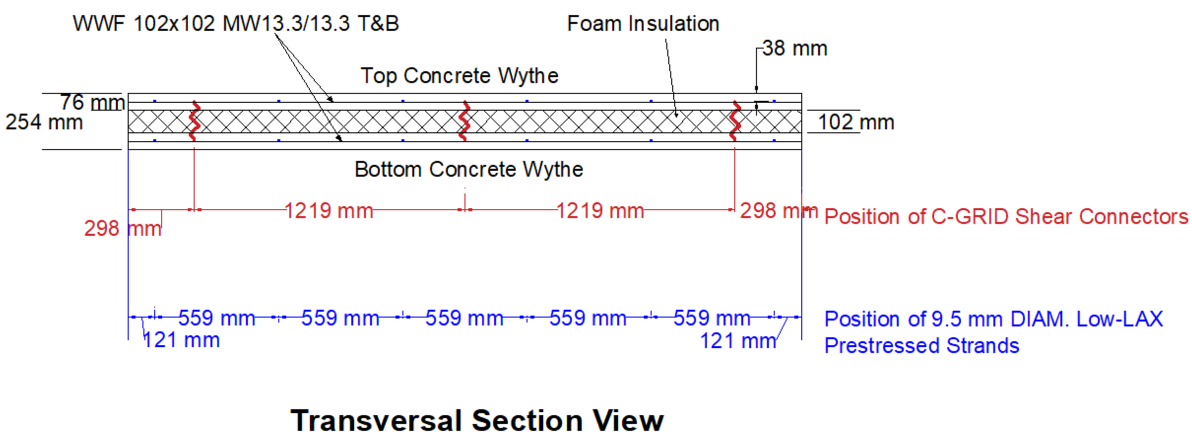

Figure 3 Transverse section of the test panel

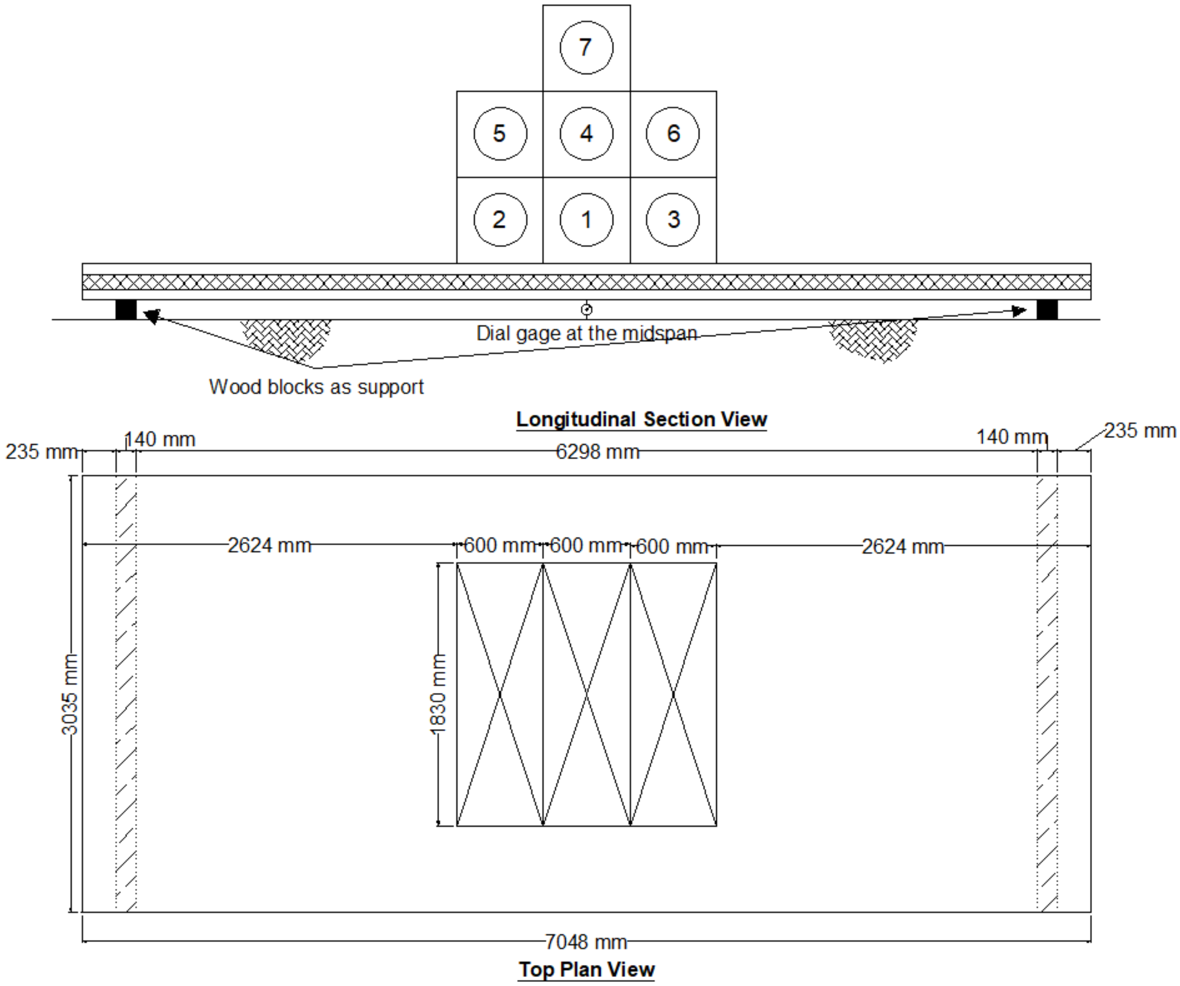

Figure 4 Test setup: (a) Longitudinal Section View; (b) Plan View

Figure 5 Final load placement

The summary of the loading and deflections are shown in Table 3 and Figure 6. As the load increased on the sandwich panel, the tensile force in the prestressing strands increased until it cracked the concrete that acted as anchorage for the strands, causing the splitting crack to develop in the concrete, as shown in Figure 7. The bottom concrete wythe had near-uniform and symmetrical transverse cracks as shown in Figure 8. The symmetrical typical bending cracks validates the use of the concrete blocks to simulate typical floor loading system. The popping of the anchorage of the shear connector was never heard and complete failure never occurred.

Table 3 Test panel load and deflection data

Block number	Block weight (kg)	Total load (kg)	Displacement (mm)
0	0	0	0
1	1542	1542	1.6
2	1542	3084	3.2
3	1565	4649	6.4
4	1542	6192	11.1
5	1107	7298	15.9
6	1166	8464	28.6
7	1107	9571	39.7

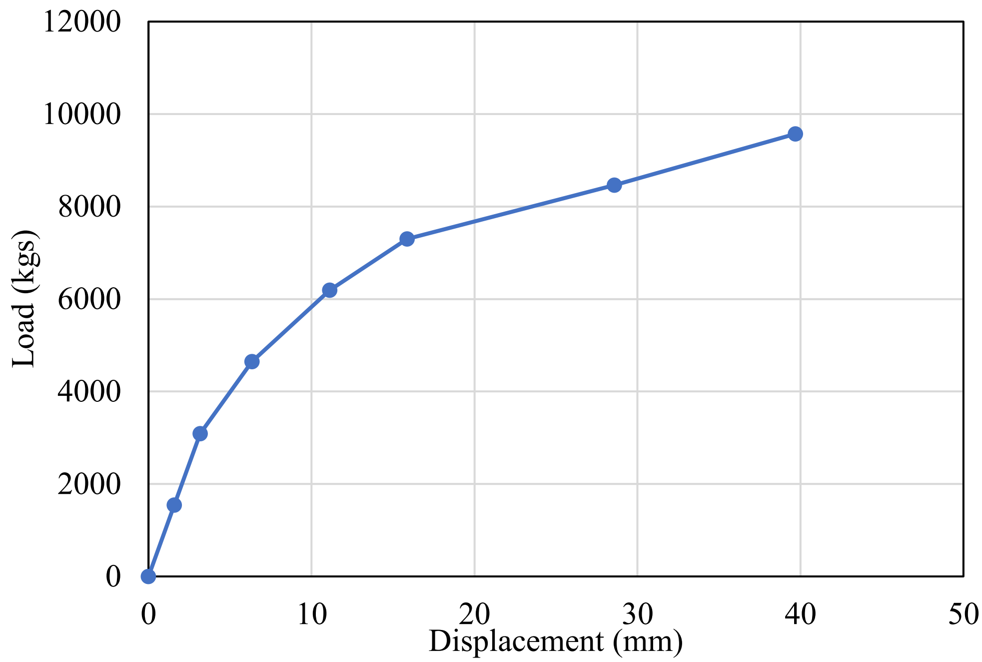

Figure 6   Load-deflection curve for the tested panel

Figure 7   Cracking of top layer concrete around longitudinal prestressing strand

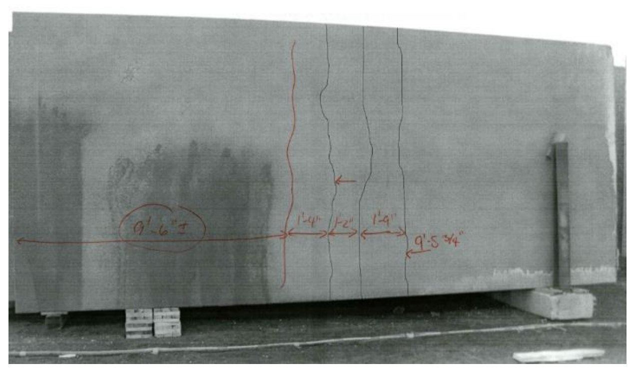

Figure 8   Uniform and symmetrical bottom transverse cracks

3. Finite Element Analysis

A Finite Element (FE) model is developed and validated with the tested panel using commercial FE analysis software package ABAQUS (2018). This FE model takes into account nonlinear material properties, concrete damage model and induced stresses from prestressing strands. The use of the concrete damage plasticity model in ABAQUS can detect the behavior of the concrete in the cracked sections, which can be used to evaluate DCA at the nonlinear stage. ABAQUS CAE module is used as a graphical user interface to facilitate the creation of the model and extraction of post-processing data.

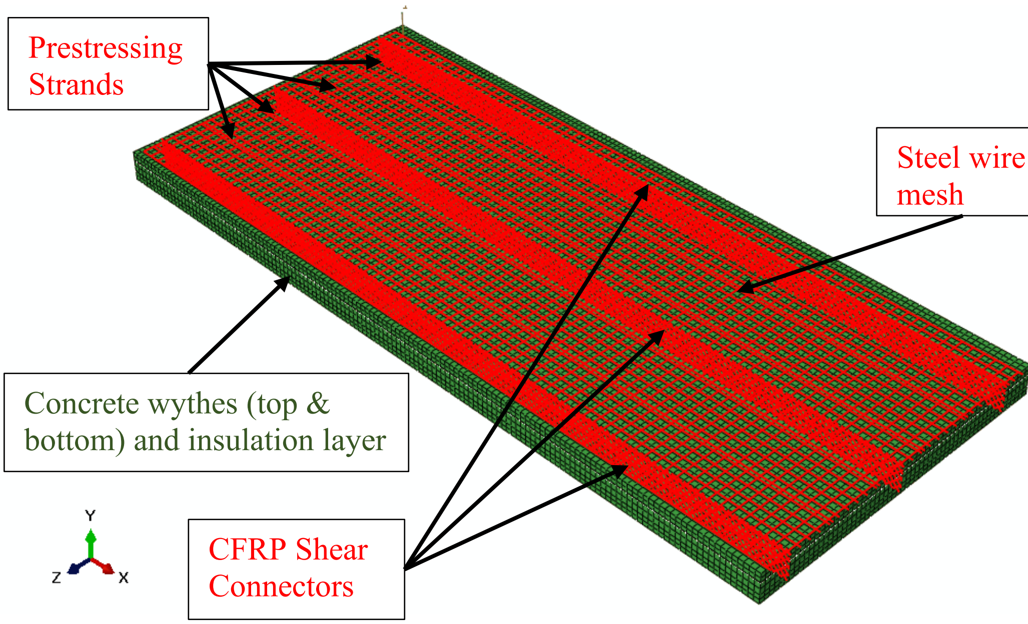

Figure 9 FE model of the test panel

3.1 Geometry

The model consists of five parts: concrete wythes, insulation layer, prestressing strands, steel wire mesh, and CFRP shear connector, as shown in Figure 9. Linear hexahedral element with enhanced stiffness hourglass control and reduced integration C3D8R is used to model the concrete and insulation. Three-dimensional linear truss element with two nodes T3D2 is used to model prestressing strands, steel wire mesh, and shear connector. The insulation layer is connected to the concrete wythes using surface tie connection, and the prestressing strands, steel wire mesh and shear connectors are embedded in the concrete using the “Embedded Element” command. Based on a convergence study that will be discussed in detail in Section 4, 50.8 mm mesh size is used in the FE model for concrete, insulation, prestressing strands, and steel wire mesh. As for the shear connector, the mesh size is based on the intersection between the strands as shown in Figure 10.

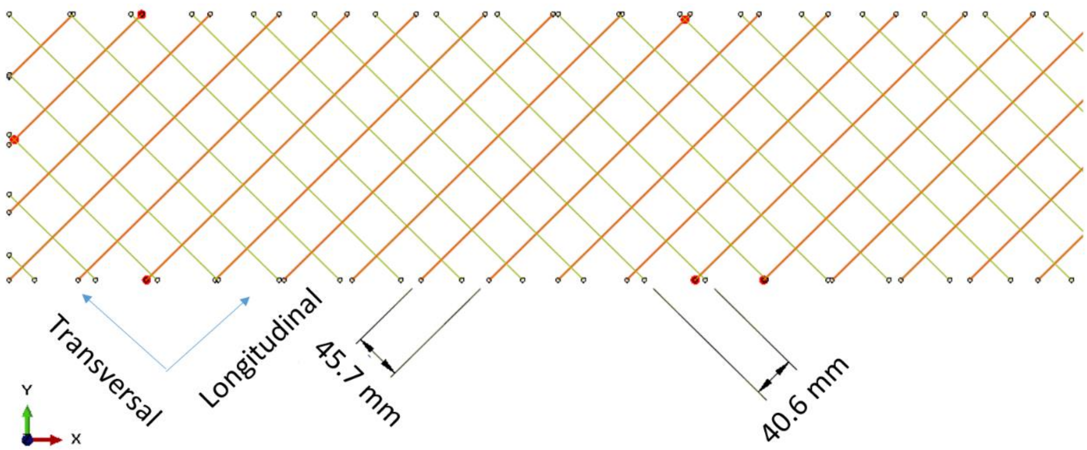

Figure 10 CFRP shear grid in the FE model

3.2 Material properties

To accurately simulate the insulated concrete sandwich test panel in the FE model, elastic and inelastic engineering properties are needed for concrete and steel components of the structure. Elastic material properties are shown in Table 1, while inelastic material properties can be obtained through existing mathematical models as will be discussed in the following sections.

3.2.1 Concrete

ABAQUS offers three modeling techniques for nonlinear concrete FE analysis. The concrete damaged plasticity model developed by Lubliner et al. (1989) and Lee and Fenves (1998) is used for the FE modeling in this study as it incorporates both the compressive and tensile properties of the concrete material. Corresponding stiffness degradation values, or damage parameters, and tension stiffening are also considered in the damaged plasticity model. This damage model is recommended by ABAQUS for concrete flexural member analyses, which suits the study well.

3.2.1.1 Concrete compressive behavior

The behavior of concrete depends on many parameters such as material properties; its interaction with other materials such as steel and fiber; the type of loading: static or dynamic; and boundary conditions such as confined or unconfined. Many mathematical models were developed to account for the aforementioned parameters based on linear and nonlinear elasticity, fracture mechanics, and hardening plasticity. However, these models are formulated in terms of the tensorial relation between stress and strain. Consequently, closed-form expressions are required to obtain a stress-strain response based on parameters such as compressive strength and elastic modulus. Several researchers have developed empirical equations, including Collins et al. (1993), Hognestad et al. (1955), Hsu and Hsu (1994), Kent and Park (1971), Popovics (1973), Roy and Sozen (1965), and Saatcioglu and Razvi (1992). In this study, Hsu and Hsu's model is used as it can generate the stress-strain relationship using only the concrete compressive strength at 28 days, and is compatible with both normal and high strength concrete. As shown in Figure 11, the concrete compressive behavior under uniaxial compression follows a linear stress-strain curve according to Hooke's law, then Hsu and Hsu's model is used for nonlinear stage starting from yielding point at $0.5\sigma_c$ until the end of the softening part at $0.3\sigma_c$, which can be calculated as follows:

$$\sigma_c = \left(\frac{\beta(\varepsilon_c / \varepsilon_0)}{\beta - 1 + (\varepsilon_c / \varepsilon_0)^{\beta}}\right)\sigma_{cu} \tag{1}$$

where σ_c is the concrete compressive stress corresponding to the concrete compressive strain (ε_c); β is a shape parameter and ε_0 is the strain at the peak stress, which can be calculated as:

$$\beta = \frac{1}{1-[\sigma_c/(\varepsilon_0 E_0)]} \tag{2}$$

$$\varepsilon_0 = 1.291 \times 10^{-5}\sigma_c(\mathrm{MPa}) + 2.114 \times 10^{-3} \tag{3}$$

where σ_c is the concrete compressive stress. The initial tangential modulus, E_0, depends on the compressive strength, which can be given as:

$$E_0 = 124.31\,\sigma_{cu} + 22636\ (\mathrm{MPa}) \tag{4}$$

For the tested panel, the concrete compressive strength (σ_{cu}) was reported to be 54 MPa, which is within the model's upper limit. Table 4 shows the calculation for the compressive stress-strain data when substituting the 54 MPa compressive strength into Equations (1) through (4).

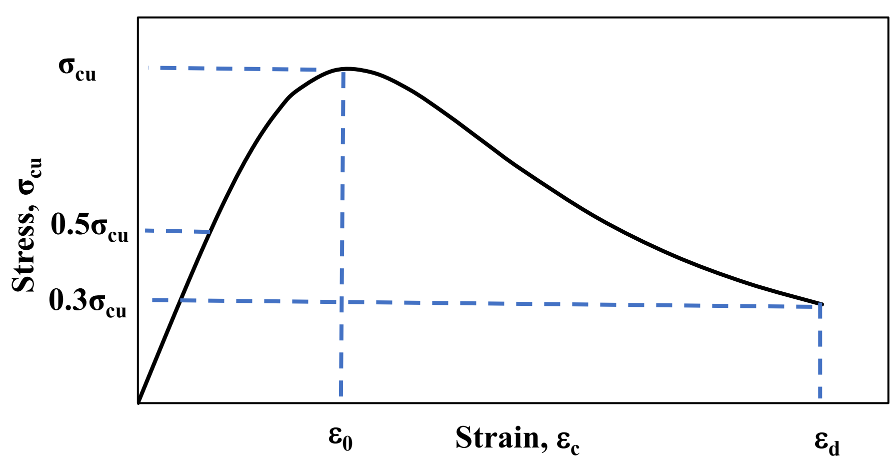

Figure 11 Typical compressive stress-strain curve

Inelastic strain (ε_c^{in}) is defined as the total strain (ε_c) minus the elastic strain corresponding to the undamaged material:

$$\varepsilon_c^{in} = \varepsilon_c - \frac{\sigma_c}{E_0} \tag{5}$$

Concrete damage is defined by Lubliner et al. (1989) where the damage factor (d) was proposed as:

$$d = 1 - \frac{\sigma}{\sigma_{\max}} \tag{6}$$

where σ_{max} is the strength of concrete. The damage factor (d) is assumed to be used only at the softening stage where the concrete stress is less than the concrete strength, as shown in Figure 12. The damage factor represents the degradation of the elastic stiffness, which is defined as:

$$E = (1 - d)E_0 \tag{7}$$

where E_0 is the initial elastic stiffness.

The damage factor is evaluated according to Equation (14) as shown in Table 4. It should be noted that ABAQUS requires the user to input the stress-strain values from the beginning of the concrete crushing region, which is shaded in Table 4. The increment of stress values is calculated so that the stress increment is less than 1% of the maximum strength to avoid numerical instability.

Table 4 Concrete compressive behavior

Maximum Compression Strength, σ_{cu}			54	MPa
Initial Tangential Modulus, E_0			29,322	MPa
Strain at Peak Stress, ε_0			0.002808	cm/cm
β-Parameter			2.8829	unitless
Linear Stage	**Strain (cm/cm) x10^{-3}**	**Stress (MPa)**	**Inelastic strain (cm/cm) x10^{-3}**	**Damage factor (d)**
	0	0	0	0
	0.92	26.9	0	0
Nonlinear stage	0.97	27.9	0.02	0
	1.09	30.8	0.04	0
	1.14	32.2	0.04	0
	1.2	33.6	0.05	0
	1.37	37.6	0.09	0
	1.48	40.1	0.12	0
	1.6	42.4	0.15	0
	1.99	48.8	0.33	0
	2.16	50.7	0.43	0
	2.33	52.2	0.55	0
	2.81	53.8	0.97	0
	3.37	52.0	1.6	0.03
	3.66	50.2	1.95	0.07
	3.94	47.9	2.31	0.13
	4.51	43.0	3.04	0.29
	4.79	40.4	3.41	0.38
	5.07	37.9	3.78	0.46
	5.92	31.2	4.86	0.66
	6.49	27.4	5.55	0.74
	7.05	24.2	6.23	0.81
	7.62	21.4	6.89	0.85
	8.47	18.0	7.85	0.89
	9.32	15.3	8.79	0.92
	10.17	13.1	9.72	0.94
	11.86	10.0	11.52	0.95

3.2.1.2 Concrete tensile behavior

Modeling of the reinforced concrete under tension loading is often known as tension stiffening, which was first introduced by Hegemier et al. (1985) to develop an analytical model to simulate the cracking of the concrete and the nonlinear responses of the steel and concrete. Since then, tension stiffening model has been developed by numerous studies including Choi and Cheung (1996), Lee and Fenves (1998), Sato and Vecchio (2003), Fields and Bischoff (2004), Nayal and Rasheed (2006), and Stramandinoli and La Rovere (2008)

Nayal and Rasheed (2006) stiffening model, which was modified by Wahalathantri et al. (2011), is used in this study to avoid convergence problems. Similar to compression behavior, implementation of tension behavior on ABAQUS requires the user to define two stages: tension stiffening and tension damage. The tension stiffening can be defined as in Figure 13, where concrete follows a linear elastic stage until its ultimate tensile strength (σ_{t0}). Then it experiences a steep degradation of stress until 0.77(σ_{t0}), which corresponds to 1.25(ε_{cr}). The stress then continues to decrease to 0.45(σ_{t0}) at 4(ε_{cr}), until it reaches 0.1(σ_{t0}) at 8.7(ε_{cr}). Cracking strain can be calculated according to Hooke's law as (σ_{t0}/E), where σ_{t0} is concrete tensile strength.

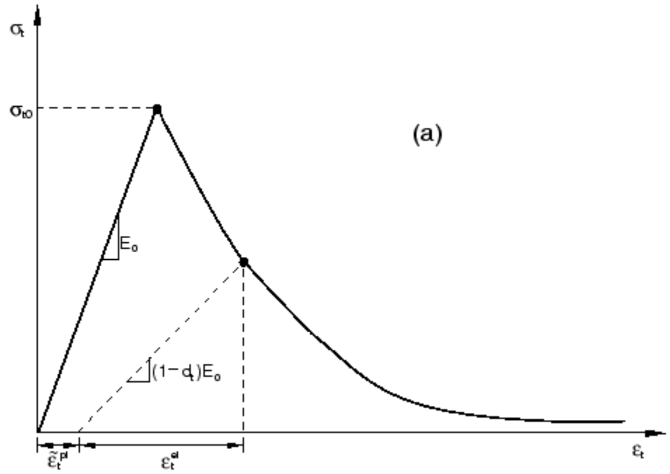

Figure 12 Tensile stress-strain response (ABAQUS, 2018)

The concrete tensile strength (σ_{t0}) can be determined based on CIB-FIP (1991) as:

$$\sigma_{t0} = 1.4\left(\frac{\sigma_{cu} - 8}{10}\right)^{2/3} \text{ (MPa)} \tag{8}$$

where σ_{cu} is concrete compressive strength. Damage model developed by Lubliner et al. (1989) in Equation (6) is used to obtain the tensile damage. The stiffening model and damage parameters are provided in Table 5.

Table 5 Concrete tension behavior

Maximum Tensile Stress, σ_{t0}				3.860	MPa
Critical Tensile Strain, ε_{cr}				0.000131639	cm/cm
Tensile Uniaxial Data		**Concrete Damaged Plasticity**			
		Tensile Behavior		**Tension Damage**	
Nominal Stress (MPa)	Eng. Strain (cm/cm)	Yield Stress (MPa)	Cracking Strain (cm/cm)	Damage Parameter (d)	Cracking Strain (cm/cm)
0.000	0	3.860	0.00	0.000	0.00
3.860	0.000131639	2.972	6.32E-05	0.230	6.32E-05
2.972	0.000164549	1.737	4.67E-04	0.550	4.67E-04
1.737	0.000526557	0.386	1.13E-03	0.900	1.13E-03
0.386	0.001145261				

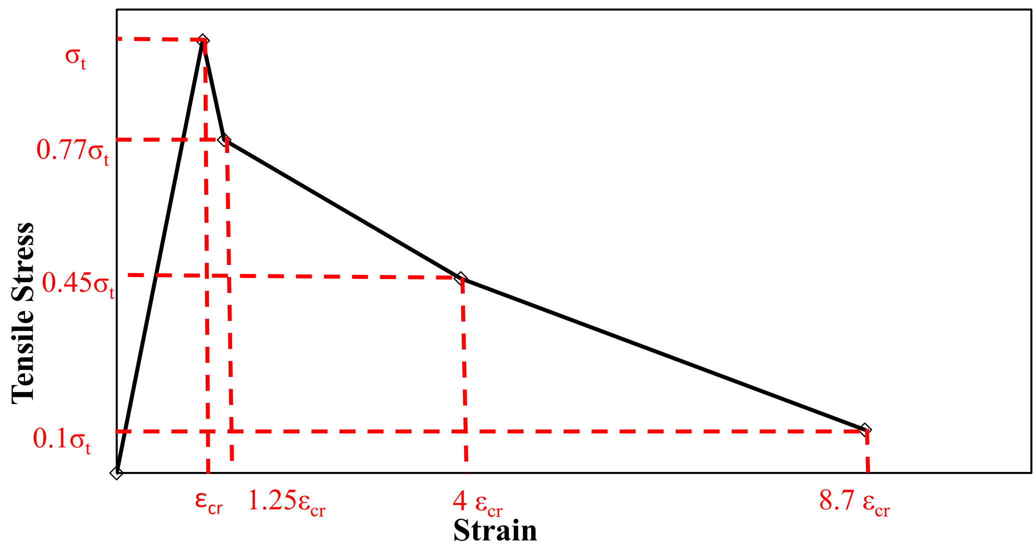

Figure 13 Tensile stress-strain curve (Wahalathantri et al., 2011)

3.2.1.3 Other concrete parameters

ABAQUS requires the user to input other concrete parameters that are related to the general behavior of the concrete. These parameters include dilation angle; flow potential eccentricity; the ratio of the initial equibiaxial compressive yield stress to initial uniaxial compressive yield stress, K_c, which is the ratio of the second stress on the tensile meridian to that on the compressive meridian; and viscosity parameter which is used for visco-plastic regularization of concrete. Some of the parameters can be obtained from the literature, and others are assumed as the default values in ABAQUS. In this study, the dilation angle is considered as 40º, $K_c = 0.667$, and the stress ratio $\sigma_{b0}/\sigma_{c0}=1.16$ as suggested by Genikomsou and Polak (2015). The flow potential eccentricity is assumed to be equal to zero, which is a default value from ABAQUS. The viscosity parameter is determined through a convergence study, which is 0.001.

3.2.2 CFRP Shear Grid Connectors

CFRP Shear connectors are used to transfer the shear between the concrete wythes. Material and section properties are calculated for both longitudinal and transversal grid elements based on Table 2 and Figure 10. Equations (9) and (10) calculate section areas for longitudinal and transversal strands, and Equations (11) and (12) calculate the strength of a single strand in longitudinal and transversal directions, respectively.

$$A_{long.} = 41.04 \times \frac{48.5}{1000} = 1.99\ (mm^2) \tag{9}$$

$$A_{trans.} = 45.4 \times \frac{45.72}{1000} = 2.03\ (mm^2) \tag{10}$$

$$f_{c-long} = 2\ GPa \times \frac{48.5}{1000} = 97\ (\mathrm{MPa}) \tag{11}$$

$$f_{c-transverse} = 1.76\ GPa \times \frac{45.72}{1000} = 80.46\ (\mathrm{MPa}) \tag{12}$$

3.2.3 Welded Wire Mesh (WWM)

Figure 14 shows the stress-strain curve for WWM adopted from Ayyub et al. (1994) for ASTM A185. The area per wire, A_{wire}, is 13.3 mm^2.

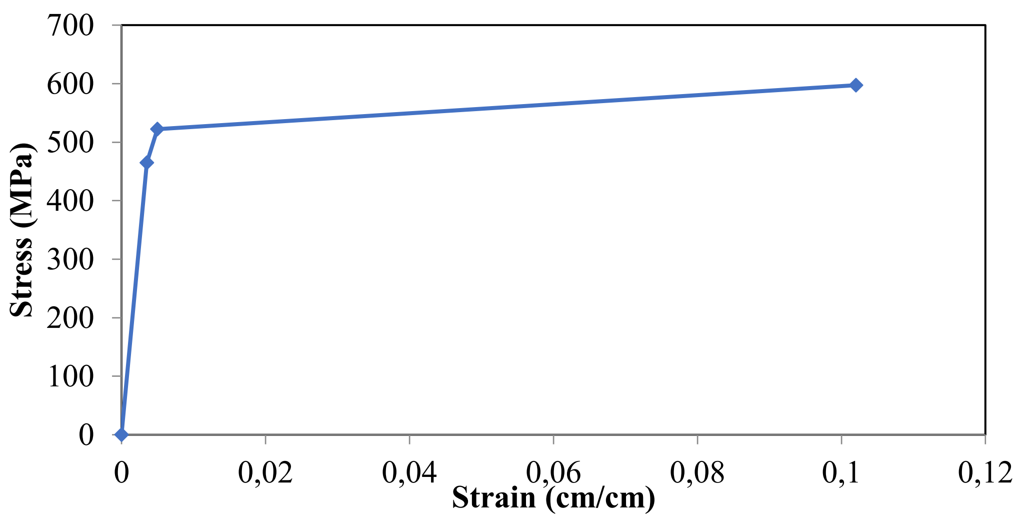

Figure 14 Constitution model for WWM [adopted from Ayyub et al. (1994)]

3.2.4 Prestressing Strands

Six Grade 270 prestressing strands with a diameter of 9.5 mm are set at 76.5 kN prestressing force and arranged over the width of the panel, with material properties summarized in Table 6.

Table 6 Material properties for Grade 270 prestressing strand

Stress Equation	Stress (MPa)	Strain (mm/mm)
f_{pi}=0.75 f_{pu}	1396.189	ε=f_{pi}/E_{ps}=0.00727
f_{py}=0.85 f_{pu}	1582.347	0.01
f_{pu}	1861.585	0.05
Notation: f_{pi}=Initial prestressing stress E_{ps}=Modulus of Elasticity of prestressing strands f_{py}=Specified yield strength of prestressing strands f_{pu}= Specified tensile strength of prestressing strands		

Initial stress provided to the strand elements is based on the values (f_{pi}) shown in Table 6. The development length is calculated according to ACI 318 (2011):

$$l_d = (\frac{f_{se}}{21})d_b + (\frac{f_{ps} - f_{se}}{7})d_b \quad (13)$$

where, f_{se} is the effective stress in prestressing strands (MPa) (after allowance for all prestressing losses), f_{ps} is the stress in the prestressing strands at nominal flexural strength (MPa). In most cases $f_{ps} \cong f_{pi}$; d_b is the nominal diameter of the prestressing strand (mm); and f_{se} can be assumed to be 1,034 MPa for grade 270 (Nawy, 2010). The strand is divided into multiple sections where each section has a length of 50 mm and a different area. Table 7 shows that the area assigned to 18 sections from each side of the strand to simulate the variation of the development length.

Table 7 Variation of the area with the strand elements for the development length

Element #	1	2	3	4	5	6	7	8	9
Area (mm^2)	1.94	7.23	12.13	16.97	21.81	26.71	31.55	36.39	41.28
Element #	10	11	12	13	14	15	16	17	18
Area (mm^2)	43.87	46.06	47.68	49.23	50.84	52.45	54.00	54.84	54.84

3.3 Loading and analysis procedure

The loads are applied through multiple steps where each step has a different load as shown in Table 3. The panel is simply supported where one support is pin and the other is a roller. Static analysis with "STABILIZE" command is used to ensure convergence.

4. Correlations between FE and Test Results

A convergence study is first conducted by varying the mesh size through 76.2 mm, 50.8 mm and 38.1 mm. Figure 15 shows the load-displacement for experimental and FE results with different mesh sizes, where good correlations can be observed between FE and test results. As shown in the figure, 38.1 mm mesh size gives the same results as those with 50.8 mm mesh but requires more than triple the simulation time. Therefore, 50.8 mm mesh is used for this study. It is worth pointing out that the displacement from the test, as shown in Figure 6, was zeroed after the panel had been set up, i.e., deflection from the self-weight of the panel was not measured in the test. The tension damage plot shown in Figure 16 matches the cracks in Figure 8.

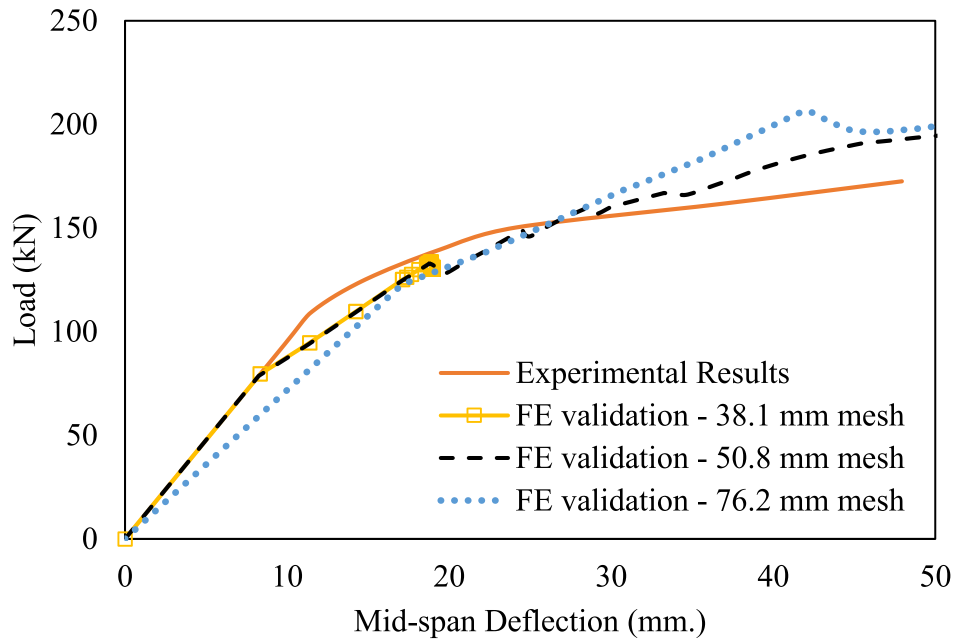

Figure 15 Load vs. deflection curves from experimental and FE analyses with different mesh sizes

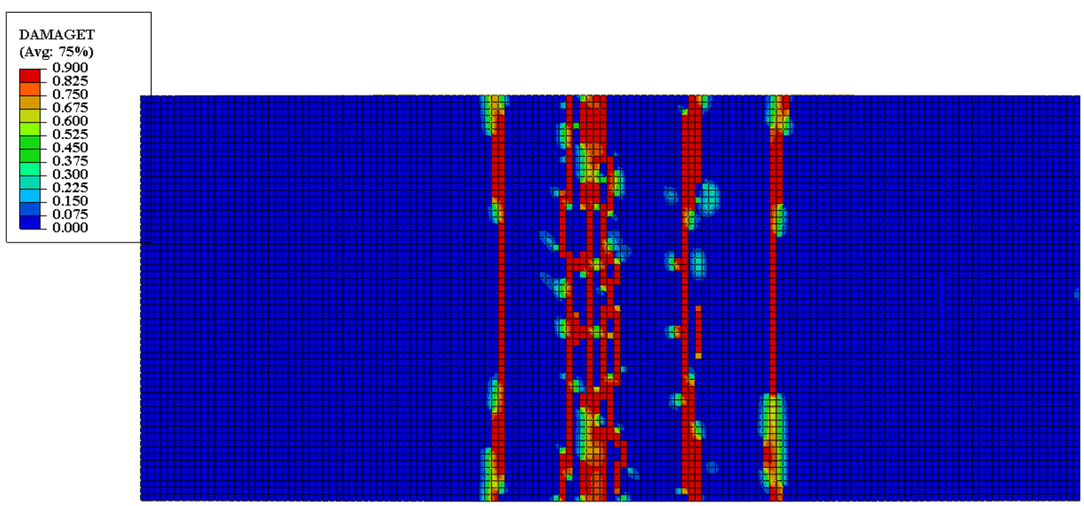

Figure 16 Bottom view of tension damage (red color represents cracked region)

5. Results and Parametric Study

A parametric study is performed to simulate DCAs varying from 0% to 100%. A solid panel with concrete replacing the insulation is modeled to provide the 100% DCA, where the shear force is fully transferred between the two layers. The authors have tried to set the stiffness of shear connector to be infinity, such as 10^7 kN/mm. The result was similar to that from the solid panel at the initial loading stage. However, they could not complete the analysis for this case due to the divergence problem caused by the localized effect. Therefore, the solid panel was used to represent 100% DCA. The 0% DCA is achieved by removing the shear grid, which will limit the longitudinal shear transfer where each layer is bending on its own. Another three models with different DCAs are chosen to expand the evaluation range.

To model different DCAs, the shear-grid is replaced by connector element "CONN3D2" with connector behavior set to Cartesian and Cardan. This element has the capability of transferring forces and rotational moments based on the stiffness provided for each Degree of Freedom (DOF). Since the main function of the shear-grid is to transfer the longitudinal shear, the stiffness of the longitudinal shear is assigned different values based on the stiffness of the shear-grid, while other DOFs are assigned as rigid. The connector element can be used directly to transfer both transitional and rotational DOF when used with shell elements. However, in the case of solid elements, the "coupling" command is needed to transfer rotational DOFs, which is configured by uniformly distributing 25.4 mm influence radius. The function of the coupling command is to control the transmission of forces through weight factors over the surrounding nodes, which is equivalent to transferring rotational DOF. The connector elements are placed between the nodes along with the locations of the shear-grid, as shown in Figure 17.

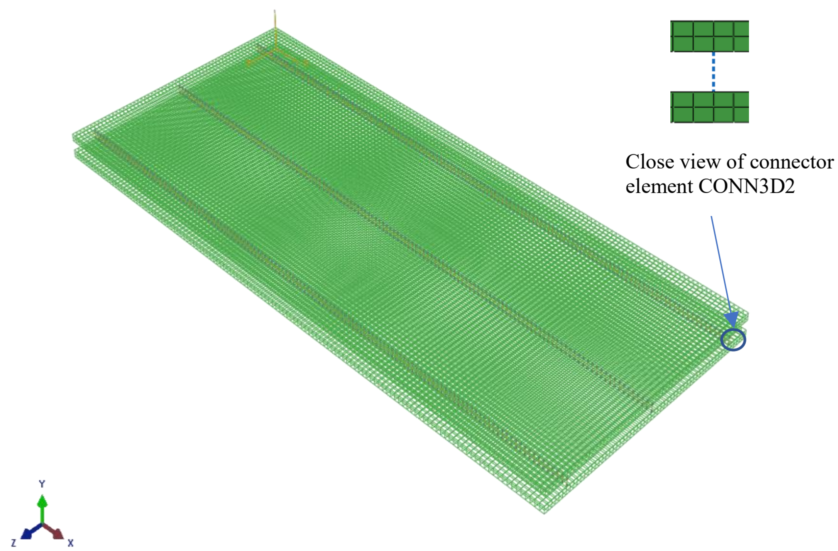

Figure 17 Sandwich panel with connectors

5.1 Displacement method

Figure 18 shows the load-displacement curves for various DCAs. DCA can be calculated using the displacement method developed by Frankl et al. (2011) as:

$$DCA(100\%) = \frac{\Delta_{noncomposite} - \Delta_{partial}}{\Delta_{noncomposite} - \Delta_{composite}} \times 100 \tag{14}$$

where $\Delta_{noncomposite}$, $\Delta_{composite}$, and $\Delta_{partial}$ represent displacements at a given load corresponding to 0%, 100%, and partial DCA, respectively. This method can only be applied to the region before yielding.

As shown in Figure 18, yield points are marked with a black hollow rounded mark, and ultimate points are marked with a black hollow triangle mark. The values of the yield and ultimate are shown in Table 9. Since the 0% DCA has the lowest yielding value (94.82 kN) and this method can only be used before yielding, DCA is evaluated at a selected load (71.2 kN) before the lowest yielding point (94.82 kN) as shown in Table 8. Other DCAs, i.e., 25%, 50% and 72% DCAs are modeled by varying the stiffness (K) of the connector elements, and they are used as a reference to evaluate other methods. Different stiffness values are shown in Table 8. It is noted that the test panel achieved a 72% DCA based on the displacement method.

It is noted that the failure load and mode of the panel depend on its DCA. As shown in Figure 18, if the DCA is high enough, the peak load could be observed, such as the case for 100% DCA. If the DCA is low, there was no obvious peak load, such as other cases in Figure 18 and the load-deflection curve in Figure 6. It is the DCA that determines the panel's behavior. If the FRP and steel connectors have the same DCA, the panels perform similarly irrespective of its connector type.

Table 8 DCAs based on displacement method

Selected load (P) (kN)	Mid-span deflection (Δ) (mm)	DCA (%)	Connector Stiffness (K) (kN/mm)
71.2	22.1	0	-
	17.0	25	0.42
	11.9	50	1.278
	7.4	72	3.5
	1.8	100	-
Dash (-) is placed in the stiffness values corresponding to 0 and 100% DCAs as they are modeled with no shear connectors and solid panel, respectively.			

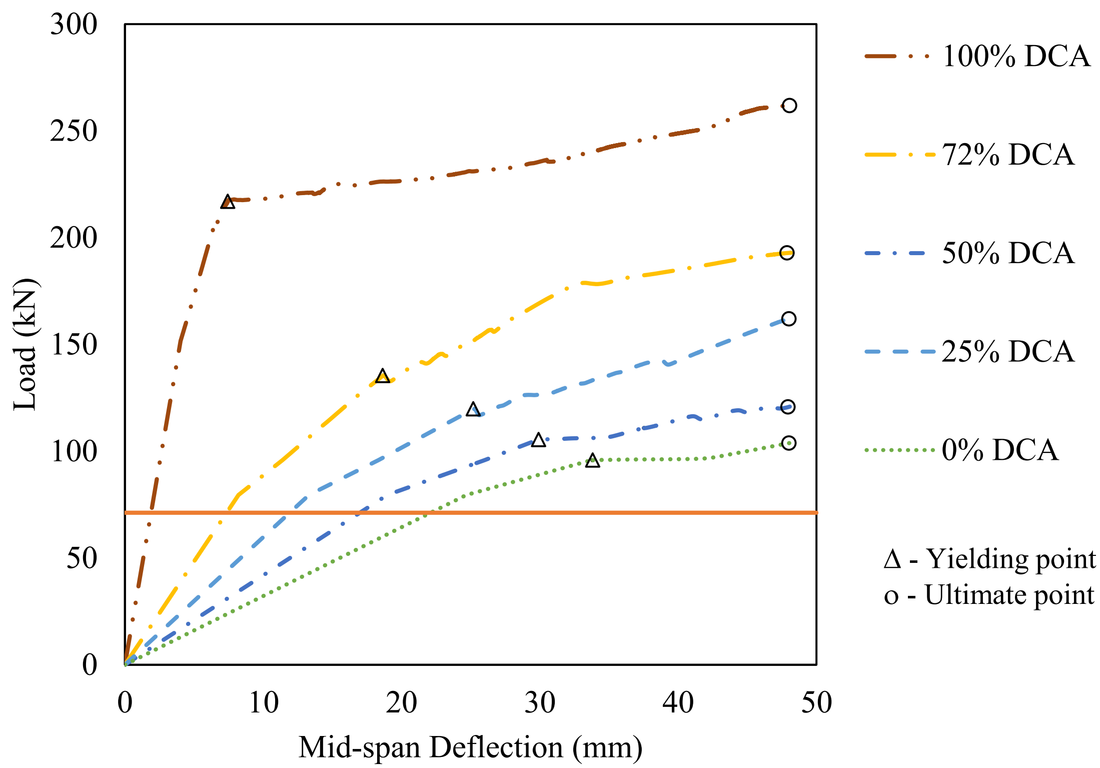

Figure 18 Load-deflection curve for different DCAs

5.2 Load method

As shown in Figure 18, for 0%, 100%, and partial DCAs, the load increases linearly with respect to displacement until the yielding point. Afterward, the load increases with respect to displacement gradually until it reaches a constant value. The DCA can be calculated based on the ultimate load for each case as:

$$DCA(100\%) = (1 - \frac{P_{composite} - P_{partial}}{P_{composite} - P_{noncomposite}}) \times 100 \tag{15}$$

where $P_{noncomposite}$, $P_{composite}$, and $P_{partial}$ represent selected loads corresponding to 0%, 100%, and partial DCAs, respectively. Table 9 shows DCAs calculated at the yield and ultimate load values for the same stiffness values used for the displacement method. It can be observed that the load method leads to different DCA values from the displacement method. Figure 19 shows that the shear transfer mechanism affects the overall behavior of the panel. As the stiffness of the shear connector increases, the stiffness of the overall panel also increases. With 0% DCA, i.e., no shear transfer, each wythe is independently subjected to tension and compression, as shown in Figure 21. This results in lower yield and ultimate load capacity. However, in the case of full composite action, i.e., full shear transfer, 100% of shear forces transfers between upper and lower wythes. The panel acts as a solid panel, which increases the yield and ultimate load capacity, as shown in Table 9.

Table 9 DCAs based on load method

K (kN/mm)	Yield disp. (mm)	Yield load (kN)	DCA (Yield load)	Ultimate disp. (mm)	Ultimate load (kN)	DCA (Ultimate load)
-	33.2	94.8	0%	48.0	103.7	0%
0.42	29,5	104.5	8 %	48.3	121.0	11 %
1.278	25.1	119.5	21%	48.3	162.1	37%
3.5	18.6	135.3	35%	47.8	192.7	56%
-	6,9	211.3	100 %	48.0	261.8	100 %
Dash (-) is placed in the stiffness values corresponding to 0 and 100% DCAs as they are modeled with no shear connectors and solid panel, respectively.						

5.3 Strain method

Strain method was proposed by Lorenz and Stockwell (1984) as shown in Figure 19 for deck slab on beam; this method can be generalized for sandwich panels as:

$$DCA = 1 - \frac{x}{x_{MAX}} \tag{16}$$

where x indicates the amount of the horizontal slip as shown in Figure 19.

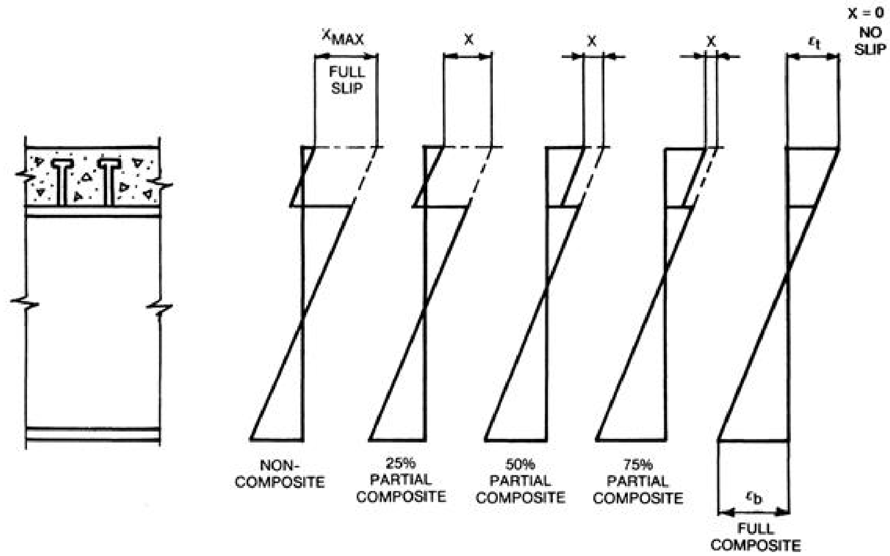

Figure 19 Partial DCA for deck slab on beam (Lorenz and Stockwell, 1984)

Equation (16) can be re-written as:

$$DCA = 1 - \frac{\varepsilon_2 - \varepsilon_1}{\varepsilon_{\max}} \tag{17}$$

where ε_1 and ε_2 are the strains for lower and upper wythes, respectively. However, for this equation to be applied to sandwich panels, the strain needs to be extrapolated to the neutral axis of the sandwich panel as shown in Figure 20.

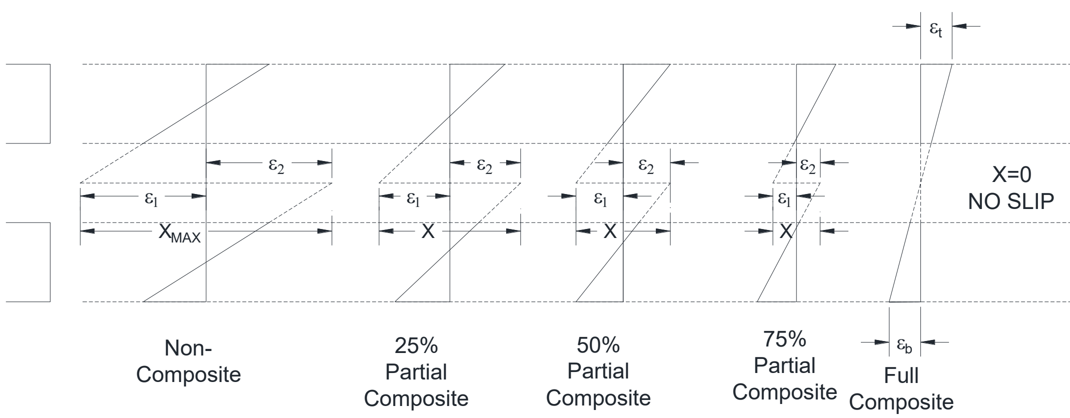

Figure 20 Partial DCA for sandwich panels

The strain in the concrete varies as the concrete properties change from elastic to plastic stage. The strain method can be used in the linear stage as the strain profile follows a linear form and can be linearly extrapolated, as shown in Figure 21. The strain values at the upper and lower wythes are exported from post-processed data at the intersection of the mid-span and the location of the edge shear connector to avoid any localized effect due to the applied loads. Two strain values are exported from each wythe since there are two elements per layer as shown in Figure 21. Once the strain profile versus the thickness is constructed, the strain values are then extrapolated to the neutral axis (127 mm) for the upper and lower layers, where the difference between the extrapolated values is calculated using Equation (17). The tested panel achieved 74% DCA as shown in Table 10, which provides similar results to the displacement method. This validates the findings from a previous study by the first author's group that DCA has a significant effect on the stress/strain induced in the sandwich panel (Yossef and Chen, 2018).

Table 10 DCA strain method calculations

K (kN/mm)	**Strain (με) at load 79.5 kN**							**DCA**
	Distance across the thickness (mm)						**Difference at 127 mm**	
	19.05	**57.15**	**127**	**127**	**196.85**	**234.95**		
-	67.24	-147.13	-540.14	412.76	19.36	-195.22	**953**	**0%**
0.42	48.39	-116.41	-418.54	290.93	-11.44	-176.37	**709**	**26%**
1.278	29.6	-85.76	-297.26	169.48	-42.14	-157.56	**467**	**51%**
3.5	12.52	-57.93	-187.08	59.21	-69.99	-140.46	**246**	**74%**
-	-7.65	-27.53	-63.97	-63.91	-100.36	-120.25	**0**	**100%**
Note: Dash (-) is placed in the stiffness values corresponding to 0 and 100% DCAs as they are modeled with no shear connectors and solid panel, respectively.								

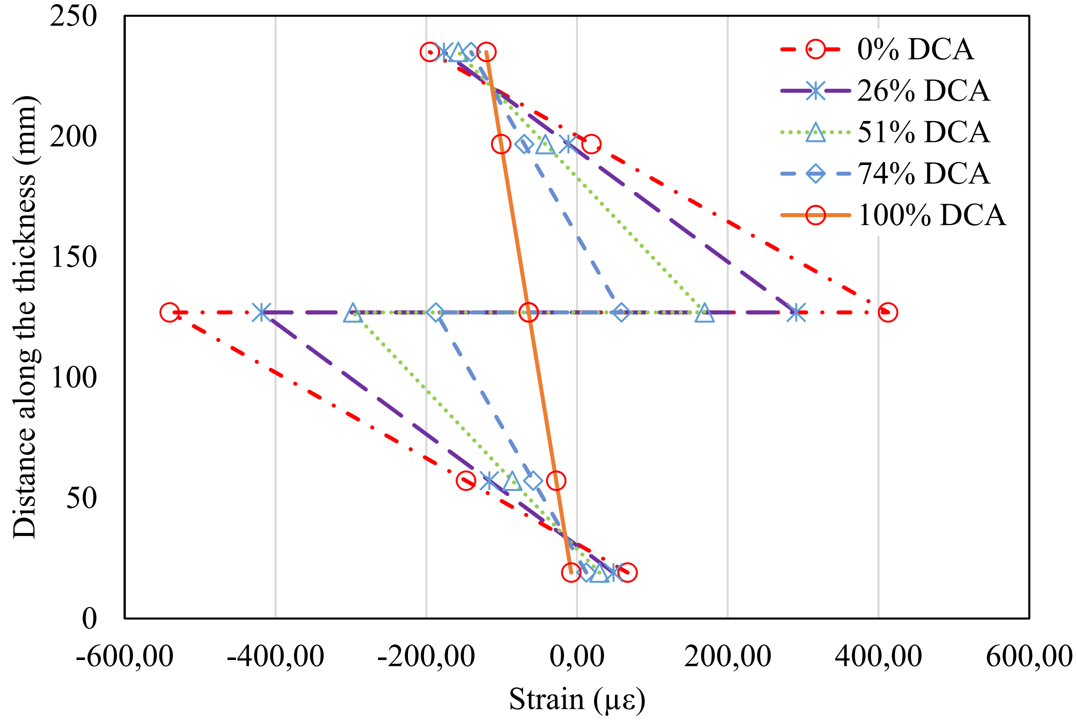

Figure 21 Strain profile at different DCAs at load 79.5 kN

6. Conclusions

A full-size panel was tested to study the behavior of the precast, prestressed insulated concrete sandwich panel with CFRP shear connectors. A FE model accounts for material nonlinear behavior, concrete damage plasticity, and prestressing force is developed, which is validated based on good correlations between the test and FE results. The FE model is further used to conduct a parametric study by varying the stiffness of the shear connectors. DCAs are then calculated and compared using displacement, load and strain methods. Based on this study, the following conclusions can be drawn:

1. CFRP shear connectors can transfer shear between concrete wythes and provide DCAs for the insulated concrete sandwich panel. Connector elements in the FE

model can provide similar behavior as the shear connectors, which can be used to evaluate different DCAs.

2. Different methods give different DCAs for the same shear connectors. The test panel achieved 72%, 35%, 56%, and 74% DCA based on displacement, yielding load, ultimate load and strain method, respectively.
3. The displacement and strain method can be used to calculate DCA in the linear region, while the load method can be used in the non-linear region.
4. Strain and displacement methods provide close results. However, the load method provides lower DCA, which can be used as a conservative method in the design.

Acknowledgment

The first author gratefully acknowledges the Science and Technology Foundation of Beijing Jiaotong University for the support (2019RC102). The second author would like to acknowledge the support from Aalto University (PostDoc/T214).

References

ABAQUS. (2018). "ABAQUS Documentation." Dassault Systèmes, Providence, RI, USA.

ACI Committee 318. (2011). *Building Code Requirements for Structural Concrete (ACI 318-08). American Concrete Institute (ACI)*, Farmington Hills, MI.

Al-Rubaye, S., Sorensen, T., Thomas, R. J., and Maguire, M. (2019). "Generalized beam–spring model for predicting elastic behavior of partially composite concrete sandwich wall panels." *Engineering Structures*, Elsevier, 198, 109533.

Ayyub, B. M., Chang, P. C., and Al-Mutairi, N. A. (1994). "Welded Wire Fabric for Bridges. I: Ultimate Strength and Ductility." *Journal of Structural Engineering*, American Society of Civil Engineers, 120(6), 1866–1881.

Bush, T. D., and Stine, G. L. (1994). "Flexural behavior of composite precast concrete sandwich panels with continuous truss connectors." *PCI Journal*, 39(2), 112–121.

Bush, T. D., and Wu, Z. (1998). "Flexural analysis of prestressed concrete sandwich panels with truss connectors." *PCI Journal*, 43(5), 76–86.

Chen, A., Norris, T. G., Hopkins, P. M., and Yossef, M. (2015). "Experimental investigation and finite element analysis of flexural behavior of insulated concrete sandwich panels with FRP plate shear connectors." *Engineering Structures*, 98, 95–108.

Choi, C. K., and Cheung, S. H. (1996). "Tension stiffening model for planar reinforced concrete members." *Computers and Structures*, 59(1), 179–190.

Choi, I., Kim, J. H., and Kim, H. R. (2015). "Composite behavior of insulated concrete sandwich wall panels subjected to wind pressure and suction." *Materials*, 8(3), 1264–1282.

Collins, M. P., Mitchell, D., and MacGregor, J. G. (1993). "Structural design considerations for high-strength concrete." *Concrete International*, 15(5), 27–34.

Comite Euro-International Du Beton. (1993). *CEB-FIP MODEL CODE 1990*. Thomas Telford Publishing.

Cox, B., Syndergaard, P., Al-Rubaye, S., Pozo-Lora, F. F., Tawadrous, R., and Maguire, M. (2019). "Lumped GFRP star connector system for partial composite action in insulated precast concrete sandwich panels." *Composite Structures*, Elsevier, 229(September), 111465.

Einea, A., Salmon, D. C., Fogarasi, G. J., Culp, T. D., and Tadros, M. K. (1991). "State-of-the-Art of Precast Concrete Sandwich Panels." *PCI Journal*, 36(6), 78–98.

Einea, A., Salmon, D. C., Tadros, M. K., and Culp, T. (1994). "A New Structurally and Thermally Efficient Precast Sandwich Panel System." *PCI Journal (Precast/Prestressed Concrete Institute)*, 39(4), 90–101.

Fields, K., and Bischoff, P. H. (2004). "Tension stiffening and cracking of high-strength reinforced concrete tension members." *ACI Structural Journal*, 101(4), 447–456.

Frankl, B. A., Lucier, G. W., Hassan, T. K., and Rizkalla, S. H. (2011). "Behavior of precast, prestressed concrete sandwich wall panels reinforced with CFRP shear grid." *PCI Journal*, Precast/Prestressed Concrete Institute, 56(2), 42–54.

Genikomsou, A. S., and Polak, M. A. (2015). "Finite element analysis of punching shear of concrete slabs using damaged plasticity model in ABAQUS." *Engineering Structures*, 98, 38–48.

Hegemier, G. A., Murakami, H., and Hageman, L. J. (1985). "On tension stiffening in reinforced concrete." *Mechanics of Materials*, 4(2), 161–179.

Hognestad, E., Hanson, N. W., and McHenry, D. (1955). "Concrete stress distribution in ultimate strength design." *Journal of the American Concrete Institute*, 52, 455–479.

Hsu, L. S., and Hsu, C.-T. T. (1994). "Complete stress-strain behaviour of high-strength concrete under compression." *Magazine of Concrete Research*, Thomas Telford Ltd, 46(169), 301–312.

Joseph, J., Prabakar, J., and Alagusundaramoorthy, P. (2017). "Precast concrete sandwich one-way slabs under flexural loading." *Engineering Structures*, Elsevier Ltd, 138, 447–457.

Kent, D. C., and Park, R. (1971). "Flexural Members with Confined Concrete." *Journal of* *the Structural Division*, 97(7), 1969–1990.

Lee, J., and Fenves, G. L. (1998). “Plastic-Damage Model for Cyclic Loading of Concrete Structures.” *Journal of Engineering Mechanics*, 124(8), 892–900.

Lorenz, R. F., and Stockwell, F. W. (1984). “Concrete Slab Stresses in Partial Composite Beams and Girders.” *Engineering Journal-American institute of steel construction*, 21(3), 185–188.

Lubliner, J., Oliver, J., Oller, S., and Oñate, E. (1989). “A plastic-damage model for concrete.” *International Journal of Solids and Structures*, Pergamon, 25(3), 299–326.

Nawy, E. G. (2010). *Prestressed concrete : A fundamental approach*. Prentice Hall, Upper Saddle River, NJ.

Nayal, R., and Rasheed, H. A. (2006). “Tension Stiffening Model for Concrete Beams Reinforced with Steel and FRP Bars.” *Journal of Materials in Civil Engineering*, 18(6), 831.

O′Hegarty, R., West, R., Reilly, A., and Kinnane, O. (2019). “Composite behaviour of fibre-reinforced concrete sandwich panels with FRP shear connectors.” *Engineering Structures*, Elsevier, 198(August), 109475.

Pessiki, S., and Mlynarczyk, A. (2003). “Experimental Evaluation of the Composite Behavior of Precast Concrete Sandwich Wall Panels.” *PCI Journal*, 48(2), 54–71.

Popovics, S. (1973). “A numerical approach to the complete stress-strain curve of concrete.” *Cement and Concrete Research*, Pergamon, 3(5), 583–599.

Roy, H. E. H., and Sozen, M. A. (1965). “Ductility of Concrete.” *Proceedings of International Symposium on the Flexural Mechanics of Reinforced Concrete, ASCE-American Concrete Institute*, 12, 213–235.

Saatcioglu, M., and Razvi, S. R. (1992). “Strength and Ductility of Confined Concrete.” *Journal of Structural Engineering*, 118(6), 1590–1607.

Salmon, D. C., Einea, A., Tadros, M. K., and Culp, T. D. (1998). “Full-Scale Testing of Precast Concrete Sandwich Panels.” *ACI Structural Journal*, 94(4), 354–362.

Sato, Y., and Vecchio, F. J. (2003). “Tension Stiffening and Crack Formation in Reinforced Concrete Members with Fiber-Reinforced Polymer Sheets.” *Journal of Structural Engineering*, 129(June), 717–724.

Stramandinoli, R. S. B., and La Rovere, H. L. (2008). “An efficient tension-stiffening model for nonlinear analysis of reinforced concrete members.” *Engineering Structures*, 30(7), 2069–2080.

Tomlinson, D., and Fam, A. (2015). “Flexural behavior of precast concrete sandwich wall panels with basalt FRP and steel reinforcement.” *PCI Journal*.

Tomlinson, D., and Fam, A. (2018). “Axial load-bending moment-interaction diagram of partially composite precast concrete sandwich panels.” *ACI Structural Journal*, 115(6), 1515–1528.

Wahalathantri, B. L., Thambiratnam, D. P., Chan, T. H. T., and Fawzia, S. (2011). “A material model for flexural crack simulation in reinforced concrete elements using

ABAQUS.” *First International Conference on Engineering, Design and Developing the Built Environment for Sustainable Wellbeing*, 260–264.

Whitehead, P. A., and Ibell, T. J. (2005). “Novel Shear Reinforcement for Fiber-Reinforced Polymer-Reinforced and Prestressed Concrete.” *ACI Structural Journal*, American Concrete Institute, 102(2), 286.

Yossef, M., and Chen, A. (2018). “A solution considering partial degree of composite action for insulated sandwich panels with general configuration flexible shear connectors.” *Engineering Structures*, Elsevier, 162(May 2017), 135–150.